Observations of Nontornadic Low-Level Mesocyclones and Attendant Tornadogenesis Failure during VORTEX*

R. J. TRAPP

NOAA/National Severe Storms Laboratory, and
Cooperative Institute for Mesoscale Meteorological Studies, University of Oklahoma, Norman, Oklahoma

19 February 1998 and 13 July 1998

ABSTRACT

Three storms intercepted during the Verification of the Origins of Rotation in Tornadoes Experiment generated a moderate-to-strong mesocyclone within the lowest several hundred meters above the ground and qualitatively appeared capable of tornadogenesis, yet did not produce a tornado. Such novel observations of what is considered ''tornadogenesis failure'' are documented and used to show the *insufficiency of a low-level mesocyclone for tornadogenesis.* Possible modes of failure are discussed.

1. Introduction

The Verification of the Origins of Rotation in Tornadoes Experiment (VORTEX; Rasmussen et al. 1994) was conducted during the spring of 1994 and 1995 in the southern Great Plains of the United States. The objectives of this validation experiment were driven by a set of hypotheses (see Rasmussen 1995) that concerned (i) the initiation of tornadic storms; (ii) low-level mesocyclogenesis, tornadogenesis, and the role(s) of mesoscale and stormscale boundaries in each; and (iii) the dynamics of tornadoes and their associated boundary layers.

VORTEX data presented herein provide additional observational basis for the sentiment expressed in Davies-Jones and Brooks (1993): ''in perhaps the least known process, a tornado develops within the mesocyclone.'' Indeed, several storms intercepted during VORTEX generated moderate to strong low-level mesocyclones that were sustained for a $\geq$15 min period,[1] and in other ways appeared ''primed for tornadogenesis'' (Brandes 1993), yet did not produce tornadoes. In other words, *existence of a low-level mesocyclone was an insufficient condition for tornadogenesis.* One may argue, then, that theories of low-level mesocyclogenesis (e.g., Rotunno and Klemp 1985; Davies-Jones and Brooks 1993; Brooks et al. 1993, 1994) fall short of explaining the details of tornadogenesis, as underscored by the idealized modeling results of Trapp and Fiedler (1995). Hence, another layer of complexity must be addressed by theories of tornadogenesis.

The aforementioned nontornadic storms are considered examples of ''tornadogenesis failure,'' an arguably subjective classification introduced here to provide a basis for comparison with tornadic storms and to help clarify tornadogenesis mechanisms. This concept of ''failure'' is attributed to Brooks et al. (1993), albeit in the context of low-level mesocyclogenesis. These authors identified failure modes in which a strong (vertical vorticity, $\zeta \sim 0.01$ s^{-1}) midlevel and/or low-level mesocyclone neither developed nor persisted in a numerically simulated storm; a failure mode was presumed to preclude the formation of a long-lived, significant tornado.[2] A proper balance between two opposing factors that govern rear-flank gust-front movement, namely the environmental inflow and the cold-air outflow, was found to be of critical importance in low-level mesocyclogenesis and sustenance [and in the sustenance of the parent storm itself; Weisman and Klemp (1982)].

The VORTEX observations imply a new challenge

[1] This approximates the minimum amount of time required to amplify, through vortex stretching with a constant divergence of -5×10^{-3} s^{-1}, vorticity of a strong mesocyclone ($\zeta \sim 1 \times 10^{-2}$ s^{-1}) to that of a tornado ($\zeta \sim 1$ s^{-1}); these vorticity and divergence values are well within the range of observed values (e.g., Lemon and Doswell 1979).

* A portion of this research was presented at the 28th Conference on Radar Meteorology, Austin, Texas.

Corresponding author address: Dr. R. Jeffrey Trapp, NSSL, 1313 Halley Circle, Norman, OK 73069.
E-mail: trapp@nssl.noaa.gov

[2] The gridpoint spacing was too coarse to resolve tornado-scale motions.

to operational forecasters in their efforts to discriminate, for warning purposes, storms that are likely to produce tornadoes from those that will not. A means to discriminate *unambiguously* between tornadic and nontornadic storms has yet to be demonstrated in the literature, hence motivating related research at the National Severe Storms Laboratory (NSSL) involving VORTEX data and complementary numerical modeling. This report provides the underpinning of some of that work by establishing existence of nontornadic low-level mesocyclones and attendant tornadogenesis failure during VORTEX.

A description of the datasets and analysis method used toward this end is provided in section 2. In section 3, evidence to support the classification of failure within three nontornadic storms is presented. A diagnostic comparison with three tornadic storms is used in section 4 to explore and provide additional clues on possible modes of failure. Some preliminary remarks on failure modes are discussed in section 5.

2. Data description

Airborne Doppler radar (ADR) observations, obtained by a helically scanning X-band radar mounted in the tail of one of the NOAA P-3 aircrafts, make up the primary data source. When employing either the fore–aft scanning technique or the all–fore, all–aft scanning technique, the P-3 is capable of gathering pseudo-dual-Doppler data during a flight leg (Jorgensen et al. 1996). A typical leg lasts ~5 min and is flown at a distance of ~10–20 km from the storm and at an altitude of ~1 km above ground level. The P-3 aircrafts also are equipped with a lower-fuselage (LF)-mounted C-band conventional radar. This radar scans at a rate of two revolutions per min and collects reflectivity information at low elevation angles with respect to the quasi-horizontal plane containing the aircraft flight track. The Weather Surveillance Radar-1988 Doppler (WSR-88D) nearest to each storm supplements the LF and airborne Doppler radars. For reference, approximate distances of these radars from the mesocyclone center of each storm, at the time of tornado formation or failure, are listed in Table 1. Details of the ADR data analysis are provided in the appendix.

The criterion for VORTEX case consideration and selection is existence of pseudo-dual-Doppler data on the storm, at least 10–15 min prior to the time of its failure. To provide a basis for comparison with tornadic storms, failure is defined to be the lack of tornado formation within a strong ($\zeta \geq 0.01$ s^{-1}) low-level mesocyclone whose life cycle is ≥15 min, and furthermore within a storm possessing other characteristics shown to be associated with a transition to a tornadic phase (Klemp 1987; see section 3). The time of occurrence of peak low-level vertical vorticity, which in these cases corresponds to the time at which tornadogenesis appears imminent (from subjective visual and/or weather radar observations) and after which low-level vertical vorticity diminishes, is designated as time of tornadogenesis failure. A tornado is defined as in the *Glossary of Meteorology*. Although each instance of tornadogenesis failure is by definition a nontornadic event, it is not assumed herein that all nontornadic storms are instances of tornadogenesis failure; ''nontornadic'' carries with it no distinction about the existence of low-level rotation, which, on some scale larger than that of the tornado, is necessary for tornadogenesis.

TABLE 1. Approximate distance (km) of each storm's mesocyclone from the airborne Doppler radar and nearest WSR-88D, at analysis time *T*. Vertical resolution is estimated for the airborne Doppler radar at the indicated range, assuming an azimuthal sampling interval or sweep-angle resolution of 1.2°. Asterisk denotes tornadic case.

Case	Distance to airborne radar (km)	Vertical data spacing (km)	Nearest WSR-88D	Distance to WSR-88D (km)
0429	14	0.29	KFWS	135
0512	10	0.21	KDDC	160
0522	16	0.34	KAMA	125
0529*	9	0.19	KFWS	155
0417*	10	0.21	KTLX	140
0516*	19	0.40	KDDC	80

WSR-88D data are used to identify times of maximum low-level rotational velocity and thus guide which ADR flight legs to analyze. Using calculations of vertical vorticity from the pseudo-dual-Doppler synthesized winds, tornadogenesis failure time is then verified, or adjusted if necessary. Additional analyses are produced at ~5 and ~10 min prior to failure time (hereinafter denoted as *T5* and *T10*).

3. Observational evidence of tornadogenesis failure

It is prudent to recall first the pioneering efforts of Stout and Huff (1953), Browning and Donaldson (1963), Chisholm and Renick (1972), Marwitz (1972), and Lemon (1980). These researchers, among others [see the reviews by Donaldson (1990) and Burgess and Lemon (1990)], introduced supercell storm airflow models and radar-observable characteristics such as pendant and hook echoes from which rotation may be inferred; bounded weak echo regions (BWER) as a means to identify regions of strong updrafts; rotation (low-altitude convergence, storm-top divergence) signatures in mean Doppler velocity that depict mesocyclones (updrafts); and spatial correlations of a mesocyclone signature and BWER that indicate a rotating updraft.

Such characteristics have been used in descriptions of supercell storm life cycles. The stage that heralds tornado formation is of relevance in the present discussion. Brandes (1993), for example, described a ''mature stage'' as ''that critical period in storm evolution at which the basic updraft and vertical vorticity patterns associated with supercells have evolved and the storm

is primed for tornadogenesis.'' A rudimentary hook echo, WER or BWER, rainy rear-flank downdraft and associated gust front, and an arc-shaped updraft that correlates spatially with vertical vorticity, are qualitative features that tend to be observed during and near the end of the mature stage. The formation of a tornadic vortex signature (TVS; Brown et al. 1978) aloft and within the mesocyclone also tends to precede tornadogenesis [though not necessarily in all cases; see Trapp and Davies-Jones (1997)]. In terms of kinematic quantities, the mature stage of the 8 June 1974 Harrah, Oklahoma, tornadic storm was characterized by $\zeta \sim 1.5 \times 10^{-2}$ s^{-1} and mean divergence of $\sim -50 \times 10^{-4}$ s^{-1}, at an altitude of 300 m (cf. Brandes 1993, his Figs. 6 and 7).

Other descriptions can be found as well. Lemon and Doswell (1979) detailed a ''collapse phase'' during which time ''the strongest tornadoes and straight-line winds occur.'' This is characterized by a dissipating BWER and the development of a divided mesocyclone structure, which are accompanied by the descent of the mesocyclone and rear-flank downdraft to the surface, and also the development of a TVS aloft. Klemp (1987) drew upon Lemon and Doswell's discussion as well as numerical storm simulation results to describe a transition of a storm to its tornadic phase. This includes a rapid increase in low-level rotation. An adverse vertical pressure gradient owing to the relatively stronger low-level mesocyclone forces a downdraft that in turn leads to the onset of mesocyclone occlusion (see also Klemp and Rotunno 1983).

With these descriptions in mind, three VORTEX cases[3] are considered herein as illustrations of tornadogenesis failure: the 29 April 1995 nontornadic storm near Sherman, Texas; the 12 May 1995 nontornadic storm near Hays, Kansas; and the 22 May 1995 nontornadic storm near Shamrock, Texas. To reiterate, a nontornadic storm that appears to evolve to a state ostensibly ''primed for tornadogenesis,'' and in particular, that possesses a moderate-to-strong mesocyclone in the lowest several hundred meters above ground, characterizes tornadogenesis failure.

Horizontal sections of reflectivity factor and storm-relative winds, at $z = 1$ km and analysis times $T5$ and T, are presented in Fig. 1.[4] Each storm exhibits, to varying degrees of intensity, a low-level mesocyclone and a rainy downdraft to its rear. An associated rear-flank gust front arcs outward from the mesocyclone center; in no storm has the gust front advanced to promote a kinematic occlusion of the mesocyclone at time T. Quasi-vertical tail radar scans of the three storms depict the presence of a deep, echo-free vault, or BWER, and therefore extensive updraft (Fig. 2a). Significant hail (diameter > 4.5 cm) was reported in each case. WSR-88D data (see Table 1) confirm a spatial correlation of WER or BWER and mesocyclone, at some time during or preceding failure. Also, data collected from the Amarillo, Texas, WSR-88D (KAMA), for example, show the presence of a TVS at $\sim$2 km above the ground within the Shamrock mesocyclone (Fig. 2b). Lastly, observations of hook echoes from the LF radar at low altitude support existence of low-level mesocyclones (Fig. 2c). Within the context of the perceived understanding of tornadogenesis, these data provide ample evidence to support the characterization of tornadogenesis failure.

LF radar data provide some clues about the nature of each storm's evolution and failure mode. In particular, scans of the Sherman storm (Fig. 2c) portray well this storm's cyclic mesocyclogenesis, and exemplify the discussions of Burgess et al. (1982) and more recently, Adlerman et al. (1996). This cyclic behavior is consistent with the evolution of the ''low-shear,'' outflow-dominated case of Brooks et al. (1994), and also with the relatively high values of radar reflectivity within the Sherman mesocyclone core.

4. Diagnostic comparison

Three tornadic storms intercepted during VORTEX now are introduced for comparative purposes: the 29 May 1994 tornadic storm near Newcastle, Texas; the 17 April 1995 tornadic storm near Temple, Oklahoma; and the 16 May 1995 tornadic storm near Garden City, Kansas. An intensity estimate (Fujita 1981) of F3 was assigned to the Newcastle tornado, F1 to the Temple tornado, and F2 to the Garden City tornado.

Prima facie, the tornadic and nontornadic storms share many of the same traits (Fig. 3). To help identify differences, several kinematic quantities[5] are computed using the radar reflectivity and three-dimensional wind analyses synthesized from the ADR. These are diagnostic, so as to show trends and ''effect'' rather than ''cause,'' yet hopefully provide further clues regarding the modes of failure. Computations using analyses that are plagued with missing data in crucial areas (e.g., in and around the mesocyclone) or that have the potential

[3] The 8 June 1995 nontornadic storm near Elmwood, Oklahoma, a VORTEX case currently under investigation by D. O. Blanchard of NSSL, also exemplifies tornadogenesis failure (D. O. Blanchard 1998, personal communication).

[4] Accounting for the approximate distance of each storm's mesocyclone from the airborne Doppler radar (see Table 1), 0.5 km is a conservative estimate of the height of the first data point above the ground level.

[5] An attempt was made to assess the magnitude and orientation of near-ground, horizontal buoyancy gradients (and therefore estimate baroclinically generated horizontal vorticity) with measurements made by a ''mobile mesonet'' [15–20 vehicles instrumented with temperature, pressure, humidity, and wind sensors at $\sim$3 m; see Straka et al. (1996)]. Unfortunately, these gradients, as anticipated by the modeling and theoretical studies of Rotunno and Klemp (1985) and Davies-Jones and Brooks (1993), were inadequately sampled by the mobile mesonet (due to poor road networks, etc.) in the cases discussed herein, at and prior to time T.

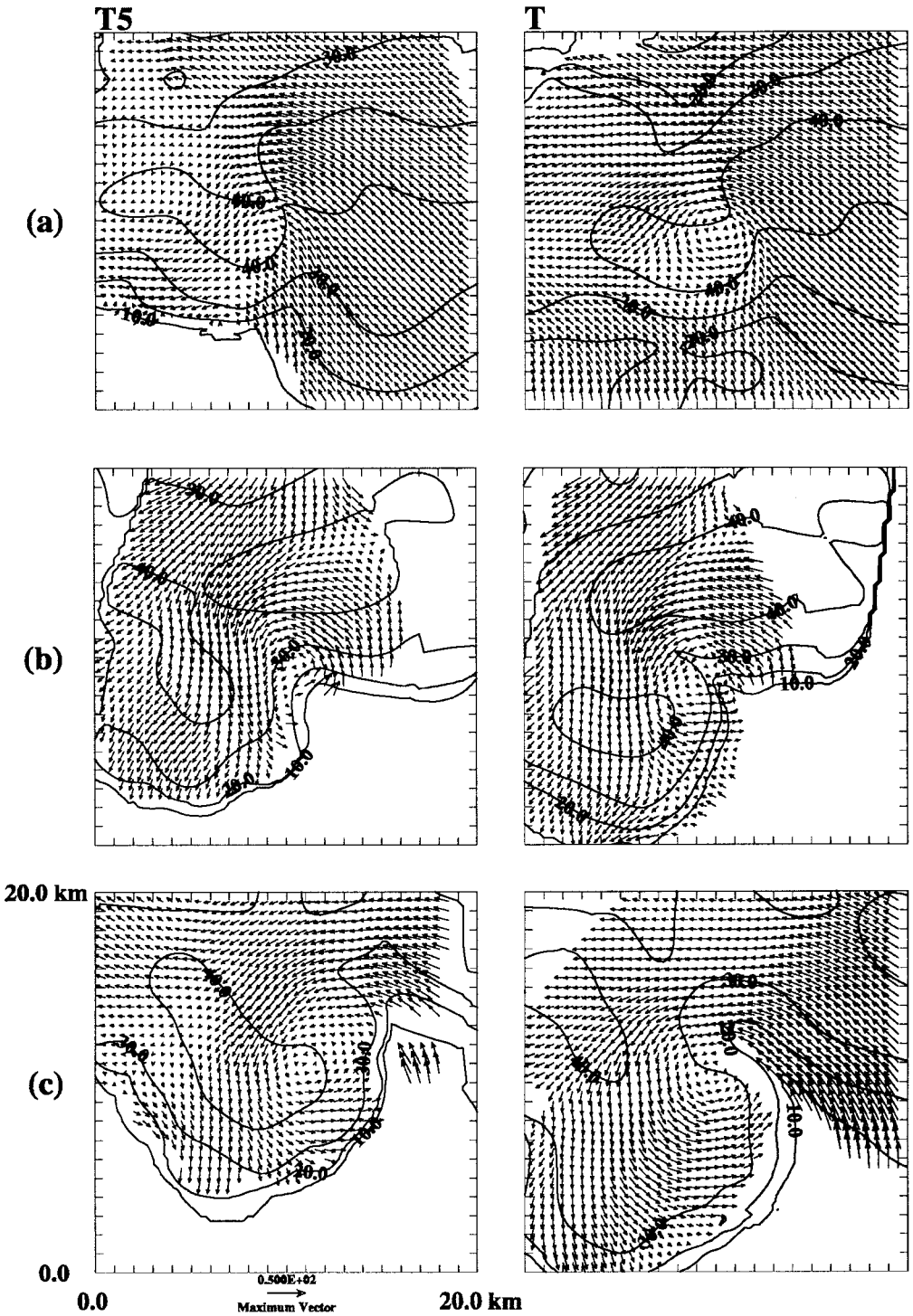

FIG. 1. Horizontal sections of storm-relative horizontal velocity and radar reflectivity factor (in dB*Z*), at 1.0-km altitude, for the nontornadic storms at analysis times *T5* and *T*. Radar reflectivity factor is contoured at 10-dB*Z* increments, and vectors are plotted at every other grid point. (a) The 29 Apr 1995 Sherman, Texas, nontornadic storm at 0023:00 (*T5*) and 0028:45 (*T*). (b) The 12 May 1995 Hays, Kansas, nontornadic storm at 2252:00 (*T5*) and 2256:20 (*T*). (c) The 22 May 1995 Shamrock, Texas, nontornadic storm at 2349:30 (*T5*) and 2358:00 (*T*). Times are in UTC unless otherwise indicated.

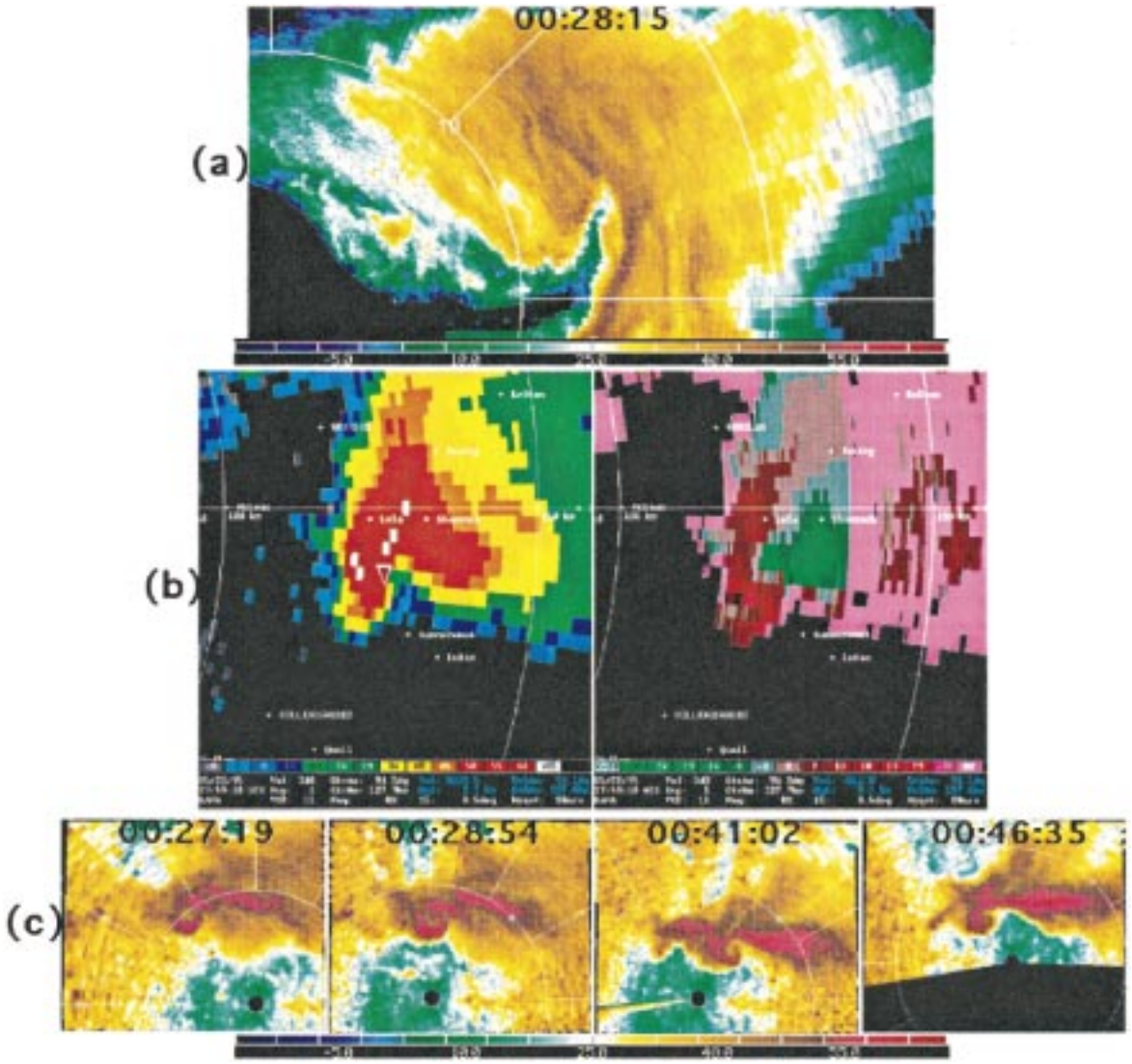

FIG. 2. Scans of (a) radar reflectivity factor (dBZ) of the 29 Apr 1995 Sherman, Texas, nontornadic storm at 0028:15, from the tail radar; (b) reflectivity and radial velocity (m s^{-1}) of the 22 May 1995 Shamrock, Texas, nontornadic storm at 2359:18, from WSR-88D KAMA at 0.5° elevation; and (c) reflectivity of the 29 Apr 1995 Sherman, Texas, nontornadic storm at 0027:19, 0028:54, 0041:02, and 0046:35, from the lower-fuselage radar.

for relatively greater vertical velocity uncertainties due to large distances between radar and storm are omitted. Accounting for errors related to the radar system hardware, flow evolution and improperly corrected storm motion during pseudo-dual-Doppler data collection, improperly dealiased velocity data, and synthesis of Cartesian velocity components from pseudo-dual-Doppler radars separated by 40° in azimuth (see Jorgensen et al. 1996), the values presented below are estimated to have errors of approximately ±10%.

It is logical to begin with an evaluation of maximum low-level ($0 < z \leq 1$ km) vertical vorticity, $\zeta_{\max}$, which is graphed for each case at each of the three analysis times (Fig. 4). Although the general trend is an increase in $\zeta_{\max}$ prior both to tornado formation and failure, the tornadic mesocyclones have greater vorticity at time T than do the nontornadic mesocyclones.

Next, consider estimates of the mean core radius, $\overline{r}_c$, within each low-level mesocyclone. Upon defining a circulation center (x_0, y_0) using $\zeta_{\max}$ and $|\mathbf{V}_H|_{\min}$, a tangential velocity can be computed:

$$V_\theta = -u \sin\theta + v \cos\theta, \qquad (1)$$

where $\theta = \tan^{-1}[(y - y_0)/(x - x_0)]$ is the azimuth angle, and u and v are the (synthesized) Cartesian velocity components. Mean core radius $\overline{r}_c$ is determined by finding the radius of maximum tangential velocity about (x_0, y_0) at each azimuth angle θ, and then averaging over θ.

In Fig. 5a, $\overline{r}_c$ is plotted as a function of $\zeta_{\max}$ at analysis

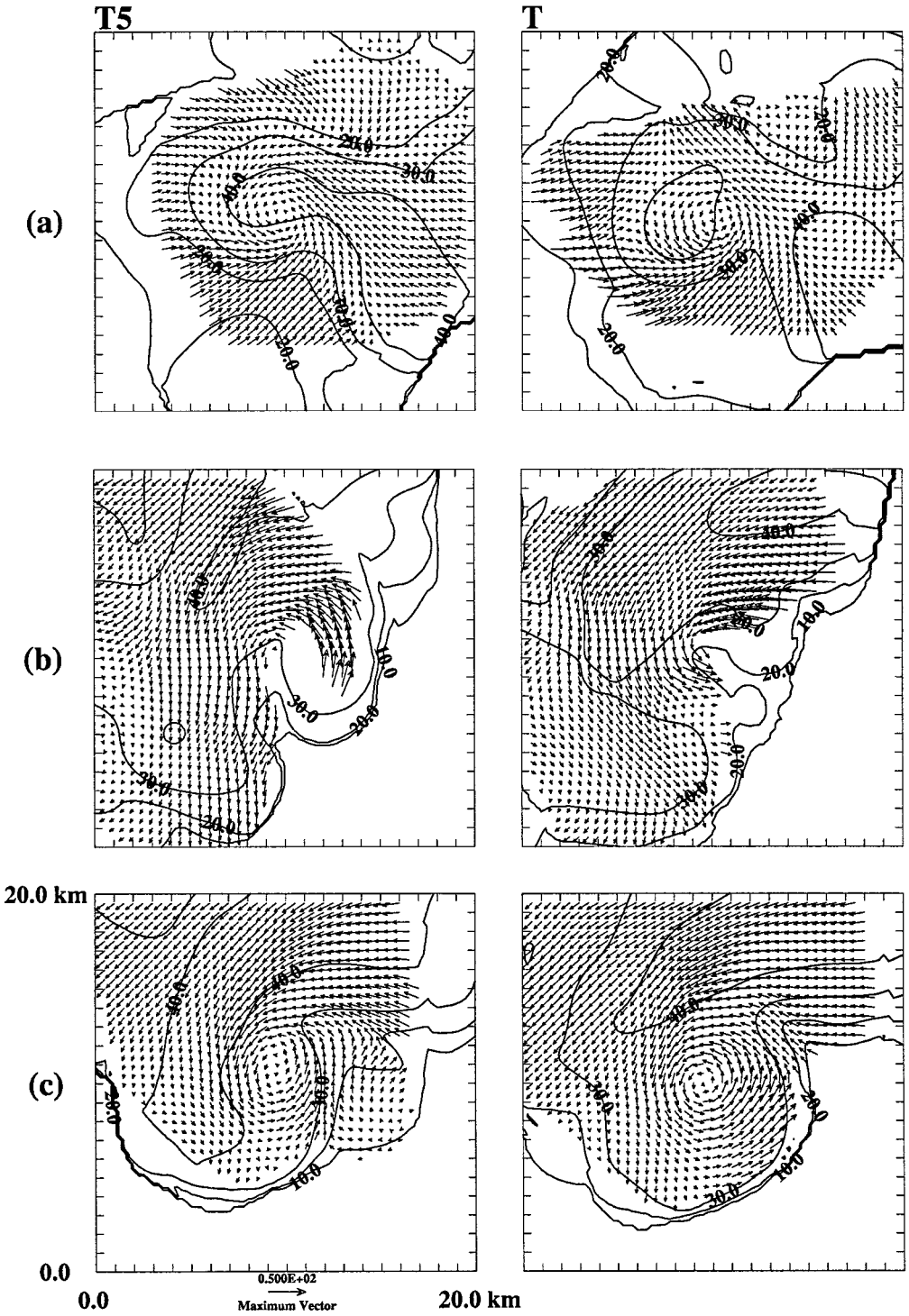

FIG. 3. As in Fig. 1 except for three tornadic storms. (a) The 29 May 1994 Newcastle, Texas, tornadic storm at 2301:15 (*T5*) and 2304:45 (*T*). (b) The 17 Apr 1995 Temple, Oklahoma, tornadic storm at 2251:52 (*T5*) and 2258:50 (*T*). (c) The 16 May 1995 Garden City, Kansas, tornadic storm at 2318:43 (*T5*) and 2324:00 (*T*).

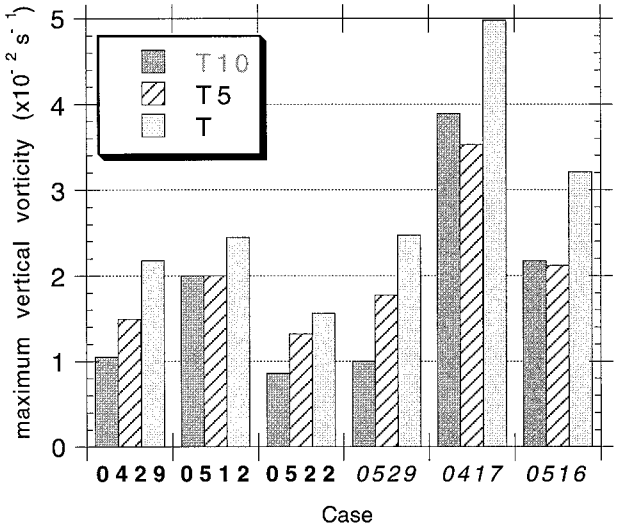

FIG. 4. Maximum, low-level ($0 < z \leq 1$ km) vertical vorticity, ζ_{max}, for each nontornadic (boldface) and tornadic (italicized) case, at the three analysis times (*T10*, *T5*, and *T*; see text).

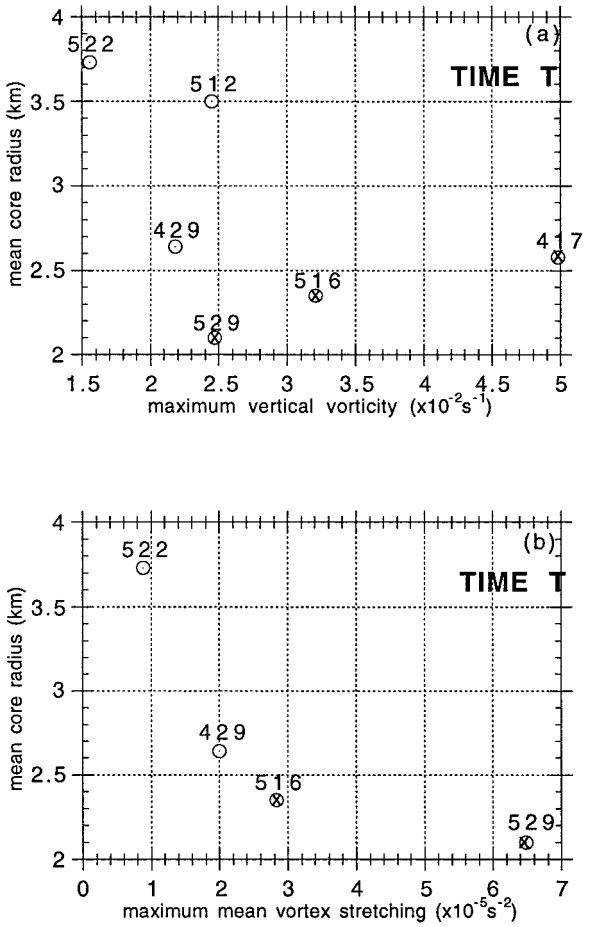

FIG. 5. Mean, low-level mesocyclone core radius $\bar{r}_c$ at analysis time *T*, as a function of (a) ζ_{max} for each case, and of (b) maximum, mean vertical vortex stretching, $-\overline{\zeta\delta}$ for two tornadic (0529, 0516) and two nontornadic cases (0429, 0512). Tornadic cases are indicated by ⊗.

time *T*. Clearly, the tornadic mesocyclones have smaller core radii and greater low-level vertical vorticity than do the nontornadic mesocyclones. This statement also holds true at analysis time *T5* and is evident qualitatively in the storm-relative winds of the Garden City (tornadic) and Shamrock (nontornadic) storms analyzed at both times (Figs. 1c and 3c).

An intuitive and theoretically consistent result is shown when $\bar{r}_c$ is plotted as a function of the maximum, mean, low-level vertical vortex stretching, $-\overline{\zeta\delta}$ (Fig. 5b). Here, δ is horizontal divergence, and the mean is constructed from all values within the nominal threshold of $\zeta > 1 \times 10^{-2}$ s^{-1}. The four cases suitable for this computation exhibit, at *T*, a well-behaved progression from large core radii and weaker vortex stretching in the nontornadic mesocyclones to smaller core radii and stronger stretching in the tornadic mesocyclones. Said another way, parcels that nearly conserve angular momentum penetrate closer to the central axis of the tornadic mesocyclones, resulting in large tangential velocities.

Correlations (or lack thereof) of vertical velocity and vertical vorticity corroborate the results in Fig. 5. Following Droegemeier et al. (1993), a correlation coefficient $\rho(w, \zeta)$ is defined at each level $0 < z \leq 1$ km as

$$\rho(w, \zeta) = \frac{\langle w\zeta \rangle}{\langle w \rangle \langle \zeta \rangle}, \tag{2}$$

where $\langle\ \rangle$ represents a horizontal average across a mesocyclone (defined by $\zeta > 1 \times 10^{-2}$ s^{-1}). Interestingly, the maximum low-level correlation decreases with time by more than 50% prior to tornado failure, yet changes very little prior to tornadogenesis (Fig. 6). This is indicative of a decoupling between low-level updraft and mesocyclone, and thus a cessation or disruption of vortex stretching.

An alternative means of diagnosing the genesis or failure in the six cases is provided through calculations of swirl ratio *S* (Davies-Jones 1973). This approach follows Brandes (1978) and Barnes (1978), who used swirl ratios computed with observed winds (by dual-Doppler radar and instrumented mesonet towers, respectively) to explain tornado development and subsequent behavior.

After Davies-Jones (1973), swirl ratio can be written as

$$S = \frac{\tan\alpha}{2a}, \tag{3}$$

where $a = h/r_0$ is the ratio of storm inflow depth (h) to nominal updraft radius (r_0). Inflow depth is approximated as in Barnes (1978) using the level of free convection (LFC) from a rawinsonde observation (raob) in the environment of each storm. As demonstrated in Fig. 7, r_0 is estimated using contoured fields of azimuthally

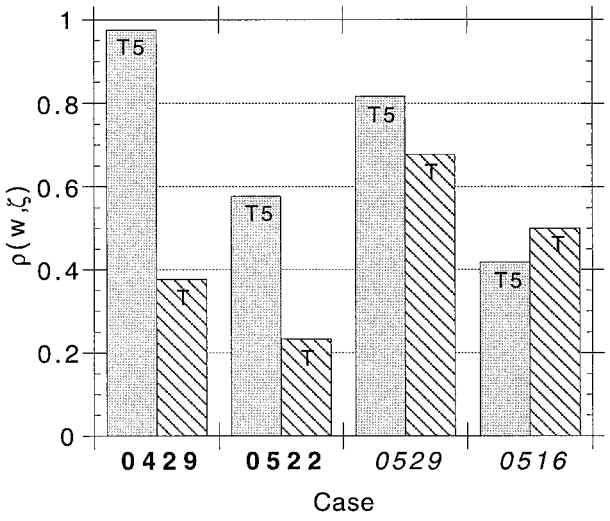

FIG. 6. Maximum, low-level correlation coefficient $\rho(w, \zeta)$ between vertical velocity w and vertical vorticity ζ, at analysis times *T5* and *T*, for two nontornadic (0429, 0522; boldface) and two tornadic (0529, 0516; italicized) cases.

averaged vertical velocity $\overline{w}$ and radial velocity $\overline{V}_r$, where

$$V_r = u \cos\theta + v \sin\theta.$$

Inflow angle

$$\alpha = \tan^{-1}(\overline{V}_\theta/\overline{V}_r)$$

is determined as in Brandes (1978) using azimuthally averaged tangential velocity [Eq. (1)] and radial velocity, evaluated at r_0 and $h/2$. Information regarding the raob for each case can be found in Table 2. Values of h, r_0, α, and S at analysis time T are listed in Table 3.

At time of tornado formation or failure, the three nontornadic storms have large swirl ratios and, with exception of the Garden City storm, the tornadic storms have smaller swirl ratios (Fig. 8). Results from laboratory model simulations as well as theory are invoked to show the consistency of large (smaller) swirl ratio with large (smaller) core radii found in the nontornadic (Newcastle and Temple tornadic) mesocyclones (see Figs. 5 and 8, and Table 3).

Turbulent vortices simulated in tornado chambers exhibit a functional dependence of core radius on swirl ratio (Davies-Jones 1973; Jischke and Parang 1974; Rotunno 1977). An inviscid, potential flow model of a stagnant core vortex aids the interpretation of the experimental data. Upon using Bernoulli's theorem and applying a variational principle, it can be shown that

$$\frac{r_{cm}}{r_0} = \frac{2SQ}{r_0^2}\left[\frac{\rho}{2(p_0 - p_c)}\right]^{1/2}, \qquad (4)$$

where r_{cm} is the minimum core radius, r_0 is the radius of the updraft hole [as in Eq. (3)], Q is the updraft volume flow rate, p_c is the constant pressure inside the stagnant core, p_0 is the constant pressure in the irrotational region outside the core, and ρ is the density (Lewellen 1976). For a fixed core pressure deficit, the core radius adjusts to its minimum value so as to maximize the volume flow rate, yet increases with increasing swirl ratio.

The stagnant vortex model does not apply at low swirl when vortices can be laminar upstream of an axial stagnation point and turbulent core (Davies-Jones 1973). However, the model and chamber experiments do well at explaining the fully turbulent vortices. In the Ward tornado chamber for example, a single, wide, fully turbulent vortex can exist in a steady state, for certain moderate values of S less than a critical swirl ratio (S^*, which is dependent on the Reynolds number, R) (see Fig. 4d in Ward 1972). Snow (1982) describes this as a vortex at ''intermediate swirl,'' the core has broadened, yet (weak) rising motion still exists along the central axis (see his Fig. 8). To the extent that such a vortex is analogous to the three nontornadic, broadly rotating mesocyclones, one may state that the swirl in these cases destines the mesocyclones to resist tornado-scale vortex formation.

This statement comes with two caveats. First, unlike in the chamber and numerical models thereof, the swirl ratio associated with the parent thunderstorm is unsteady and therefore is a manifestation of storm-scale processes at a given time. Second, the chamber/numerical models inadequately treat (and ADR observations fail to resolve) Reynolds number–dependent boundary layer processes that play an important role in tornado dynamics (see, e.g., Snow 1982). This was stressed by one of the reviewers, who noted furthermore that if these processes are simulated sufficiently well, the models may reveal certain atmospheric values of R that allow strong radial inflow to develop in the surface layer and subsequently converge the otherwise nontornadic low-level mesocyclone of an intermediate swirl vortex into a tornado. In this regard, tornadogenesis failure is dependent on R as well as S. Ultimately, the discussion of failure must relate atmospheric conditions to particular values of S and perhaps R.

The Garden City storm and its thermodynamic environment foster the formation of a two-celled mesocyclonic vortex (i.e., downflow along the central axis, terminating in low-level radial outflow that turns vertical in an annular updraft at an outer radius) that apparently exceeds some critical swirl ratio. As in laboratory vortices at $S \geq S^*$ and in multiple vortex tornadoes (Davies-Jones 1973; Jischke and Parang 1974; Church et al. 1979), a downdraft, presumably owing to a downward-directed vertical pressure gradient force, supplants upward motion along the Garden City mesocyclone's central axis at times *T10* (not shown) and *T5* (Figs. 1c and 9). According to Rotunno (1984), the two-celled vortex is unstable to three-dimensional perturbations, and the instability is manifest greatest in azimuthal wavenumber two. These subsidiary vortices form in the annular

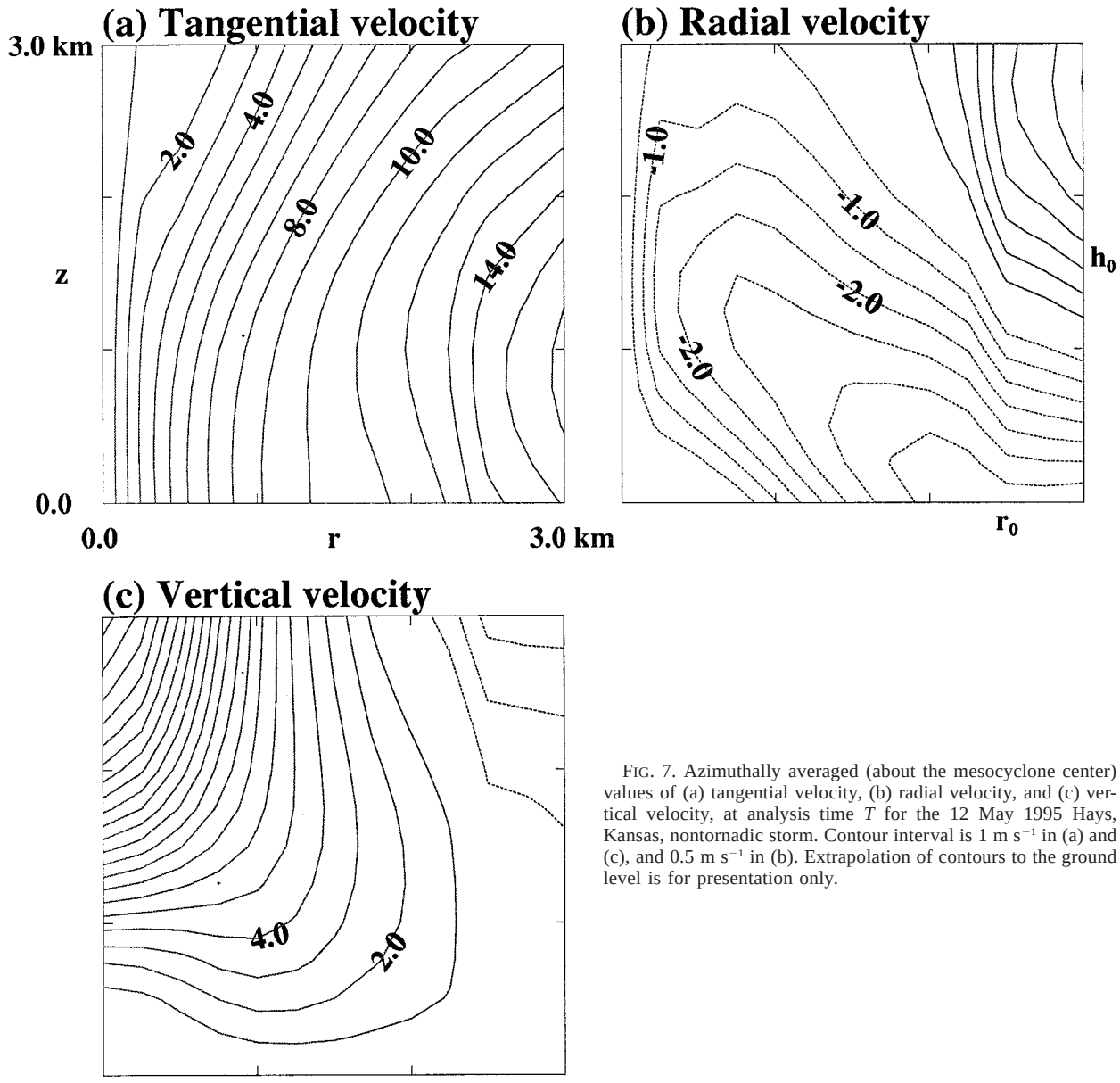

FIG. 7. Azimuthally averaged (about the mesocyclone center) values of (a) tangential velocity, (b) radial velocity, and (c) vertical velocity, at analysis time T for the 12 May 1995 Hays, Kansas, nontornadic storm. Contour interval is 1 m s^{-1} in (a) and (c), and 0.5 m s^{-1} in (b). Extrapolation of contours to the ground level is for presentation only.

TABLE 2. A few relevant details concerning the raob chosen to represent the environment of each storm. The separation distances and times are determined with respect to the mesocyclone center at analysis time T. Asterisk denotes tornadic case.

Case	Raob–storm separation time (h), distance (km)	CAPE (J kg^{-1})	LFC (km)
0429	2.5, 45.0	2630	1.5
0512	1.5, 80.3	1090	1.6
0522	3.0, 54.0	2300	2.3
0529*	0.25,130.	3380	2.0
0417*	0.33, 45.7	1810	2.3
0516*	0.3, 70.9	2470	2.3

TABLE 3. Values of storm inflow depth (h), updraft radius (r_0), azimuthally averaged tangential velocity ($\overline{V}_r$) evaluated at r_0 and $h/2$, and inflow angle $\alpha = \tan^{-1}(\overline{V}_\theta/\overline{V}_r)$, used to determine swirl ratio (S) for each case at analysis time T. Mean core radius in the ratio r_c/r_0 is as presented in Fig. 5. Asterisk denotes tornadic case.

Case	r_0 (km)	h (km)	$\overline{V}_\theta$ (r_0, $h/2$)	$\overline{V}_r$ (r_0, $h/2$)	S	$\overline{r}_c/r_0$
0429	3.0	1.5	14.0	−1.5	9.0	0.87
0512	2.5	1.6	14.0	−2.0	5.5	1.4
0522	3.5	2.3	18.0	−3.5	3.9	1.16
0529*	3.0	2.0	10.0	−3.75	2.0	0.70
0417*	4.0	2.3	6.0	−15.5	0.3	0.65
0516*	3.0	2.3	17.0	−1.5	7.4	0.96

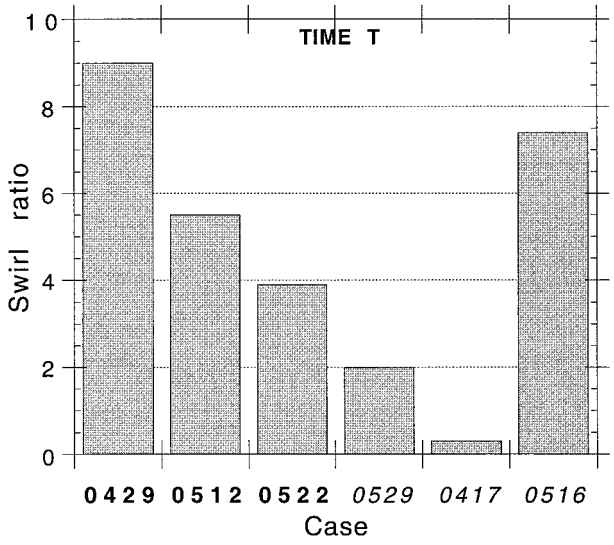

FIG. 8. Swirl ratio *S* (see text), evaluated at analysis time *T*, for each nontornadic (boldface) and tornadic (italicized) case.

updraft ring that surrounds the central downdraft (see Rotunno 1984, his Figs. 9 and 11).

Brandes (1978) and later Rotunno (1984) hypothesized that a subsidiary vortex in the two-celled mesocyclone of the 8 June 1974 Harrah, Oklahoma, storm contracted into the Harrah tornado. Wakimoto and Liu (1998) applied this theory to their analysis of the National Center for Atmospheric Research (NCAR) Electra Doppler radar data collected on the Garden City storm and tornado. Although the spatial and temporal data sampling of the NOAA P-3 data shown here are too large to afford a confirmation of Wakimoto and Liu's conclusion, it is nevertheless supported by visual observations by VORTEX personnel of tornadogenesis near the periphery of the mesocyclone rather than in its center.

5. Remarks

Six storms intercepted during VORTEX were considered. Each of the three tornadic and three nontornadic storms generated and sustained a mesocyclone in the lowest several hundred meters above the ground. Significantly, this statement proves that mere existence of a low-level mesocyclone was insufficient for tornado formation in the nontornadic cases.

The percentage of low-level mesocyclones associated with tornadoes has yet to be presented in the formal literature; it is presumed to be greater than 30%–50% [the approximate number of tornadic midlevel mesocyclones; Burgess and Lemon (1990)], but less than 100%. Assuming that detection of a low-level mesocyclone (when possible) weighs heavily in Doppler-radar-based tornado warning decisions, these observations of nontornadic low-level mesocyclones introduce another uncertainty to the decision process, and complicate the tornadic/nontornadic storm discrimination problem.

It is possible to speculate on a number of tornadogenesis failure modes that can be addressed in future studies. Certainly, a storm that becomes ''outflow-dominated'' exemplifies one mode. As discussed in Brooks et al. (1993, 1994), the processes that give rise to low-level mesocyclogenesis also disrupt the subsequent intensification of associated low-level vorticity into a tornado-scale vortex. This means of failure presumably is quite time sensitive. Noting the analyses presented in sections 3 and 4, it is clear that not every nontornadic storm ''fails'' via mesocyclone undercut by cold-air outflow.

Recall the distinct modes of tornado formation within a single-celled mesocyclone, as described by Trapp and Davies-Jones (1997): (i) mode I, in which the embryonic tornado develops aloft within the parent mesocyclone, then gradually descends to the ground via a process known as the ''dynamic pipe effect'' (Leslie 1971); (ii) mode II, in which the embryonic tornado forms uniformly throughout a several kilometer depth or very near the ground, then contracts rapidly into a tornado. Both have corresponding failure modes. Mode I should fail if the vertical stability in the convective boundary layer is too large. The result is an embryonic tornado suspended above the ground. Mode II should fail if the primary meridional (radial–vertical) circulation associated with the updraft is too weak, particularly at low altitudes, to contract ambient rotation (the mesocyclone) into a tornado within tens of minutes. This also may be interpreted as a cause for the intermediate swirl vortex, which resists tornado-scale vortex formation (for certain values of Reynolds number, as discussed previously). The primary meridional circulation is driven in part by buoyancy forces, the vertical integral of which corresponds to the convective available potential energy (CAPE), and also by upward-directed vertical pressure gradient forces (VPGFs) owing to interactions between the updraft and ambient wind shear. Following recent results of McCaul and Weisman (1996), it is suspected that these favorable VPGFs and also the height of maximum positive buoyancy are more relevant to failure mode II than the value of CAPE alone.

The frequency with which tornadoes develop within two-celled mesocyclones is unclear, as is the frequency of two-celled mesocyclone formation itself. It is reiterated that the critical swirl ratio S^*, the theoretical value at which two-celled vortices develop, is a function of Reynolds number and should vary from storm to storm. Inability of the storm to attain S^* represents in some sense yet another mode of failure. Meteorological conditions in the near-storm, mesoscale environment (which perhaps include the effects of neighboring or preexisting storms) modulate this and the other failure modes in ways yet to be determined.

Much of the data collected during VORTEX lack the spatial and temporal resolution needed for a rigorous

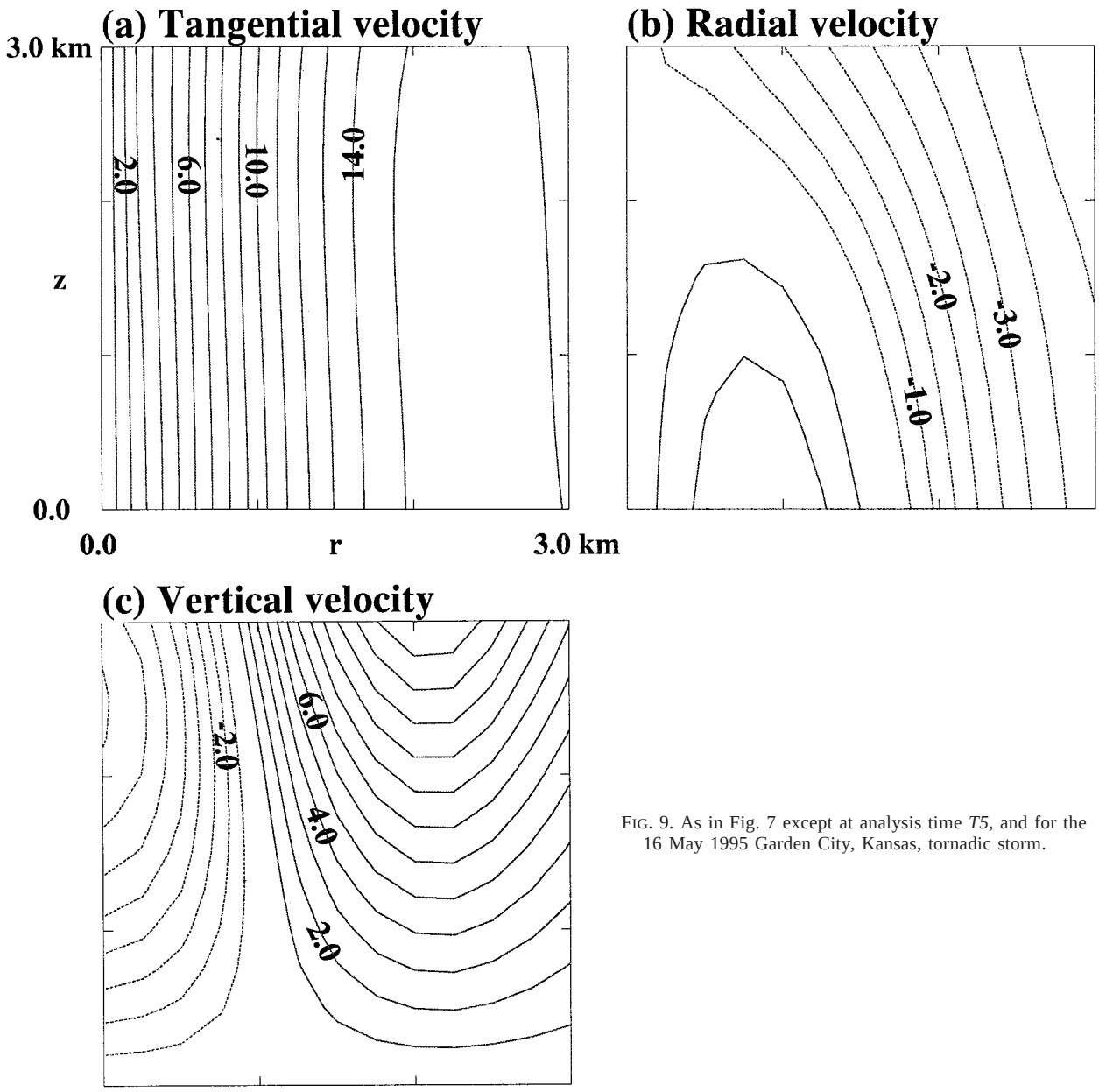

FIG. 9. As in Fig. 7 except at analysis time *T5*, and for the 16 May 1995 Garden City, Kansas, tornadic storm.

investigation of these and other conjectured failure modes. Thus it is premature at this time to attempt to assign a particular mode to a given storm. The investigative problem is, however, amenable in many ways to experiments with a numerical cloud model since tornadogenesis failure ultimately is related to meteorological conditions in the near-storm, mesoscale environment, as just mentioned. This likely will be the future direction of the research theme introduced here, in what can be considered a logical extension of the work of Brooks et al. (1994).

Acknowledgments. The author is grateful to H. Brooks, C. Doswell, E. Rasmussen, T. Shepherd, I. Watson, and C. Ziegler (NSSL), for assistance and enlightening discussions on this research. The author also benefited from comments by the two reviewers and conversations with D. Dowell, S. Weygandt, and J. Wurman (University of Oklahoma). R. Davies-Jones (NSSL) is recognized for suggesting and helping interpret the swirl ratio calculations and also serving as the author's mentor while a National Research Council–NOAA Postdoctoral Research Associate. Funding and support for VORTEX

field operations were provided by NOAA/NSSL, Center for the Analysis and Prediction of Storms at the University of Oklahoma (NSF ATM 912-0009), and the Graduate College at the University of Oklahoma.

APPENDIX

Airborne Doppler Radar Analysis Method

The airborne Doppler radar data analysis begins with a mapping from an aircraft-relative coordinate system to an earth-relative coordinate system, as well as a correction for aircraft motion applied to the radial velocity. These are derived by Lee et al. (1994) and performed using software developed by Oye et al. (1995). Because of infrequent updates of latitude and longitude by the onboard computer, it is also necessary during postprocessing to correct the latitude and longitude stored in each radar beam data header (E. Rasmussen 1996, personal communication). Reflectivity and velocity data are then edited manually with NCAR's Research Data Support System to remove ground clutter and other spurious echoes. Further editing of aliased velocity values is required due to the relatively low (12.88 m s^{-1}) unambiguous velocity. In the middle and upper portions of most of the storms, severe speckling (see Wakimoto and Atkins 1996) of the radial velocity precludes velocity dealiasing. Thus, subsequent data processing is restricted to the lowest several kilometers of the storm. Despite placing limitations on techniques for vertical integration of the continuity equation (see below), a truncated vertical domain suffices for the current objectives since the pseudo-dual-Doppler analyses are used primarily for computation of kinematic quantities at low altitudes; WSR-88D data are used for interpretation of mid- and upper-level storm structure.

Interpolation of the edited data to a 20 km $\times$ 20 km $\times$ 3 km Cartesian grid of 0.25-km spacing is performed with a single-pass, Barnes objective analysis scheme (Barnes 1964). A dimensional smoothing parameter (see Koch et al. 1983) value of 1.866 km^2 is used. This corresponds to a theoretical spectral response of 0.01 for a 2-km scale (which is considered 2Δ or the minimum resolvable scale, based on the *largest*[6] of the typical along-track scan separation distance or vertical datapoint spacing affecting the analysis domain). Though dependent on the radar rotation rate, nominal P-3 ground speed, and scan strategy, a typical value of the along-track separation distance is 0.7 km (see Jorgensen et al. 1995). Estimates of the vertical datapoint spacing at the range of mesocyclone center are provided in Table 1.

During the interpolation step, datapoint positions are corrected for storm motion as recommended by Gal-Chen (1982), except here a mean motion derived from the mesocyclone track over a 30-min period is used. Errors in the wind synthesis that are associated with storm *evolution* are not correctable. These arise because of the time lag between the fore and aft beam pair comprising a pseudo-dual-Doppler observation at a point.

Cartesian velocity components (u, v) are synthesized from the radial velocities of the fore and aft scans in a manner similar to that outlined in numerous articles (e.g., Brandes 1977; Ray et al. 1980). Vertical velocity (w) is determined from the anelastic continuity equation, using an explicit technique discussed by Gal-Chen (1983, unpublished manuscript), Sperow (1995), and Sperow et al. (1995). The integration is taken from the ground (where w is assumed to be zero) upward; errors in w accumulate with increasing height, but do not reach severe levels because of the relatively shallow domain height of 3 km. The interested reader is referred to Ray et al. (1980) for estimates of vertical velocity error variances due to upward integration of the continuity equation.

[6] In a few cases, the minimum resolvable scale is less than 2 km, but the use of a different smoothing parameter for different cases would lead to an inconsistent comparison.

REFERENCES

Adlerman, E. J., K. K. Droegemeier, and M. Xue, 1996: Numerical simulations of cyclic mesocyclogenesis. Preprints, *18th Conf. on Severe Local Storms,* San Francisco, CA, Amer. Meteor. Soc., 728–732.

Barnes, S. L., 1964: A technique for maximum detail in numerical weather map analysis. *J. Appl. Meteor.,* **3,** 396–409.

——, 1978: Oklahoma thunderstorms on 29–30 April 1970. Part II: Radar-observed merger of twin hook echoes. *Mon. Wea. Rev.,* **106,** 685–696.

Brandes, E. A., 1977: Flow in a severe thunderstorm observed by dual Doppler radar. *Mon. Wea. Rev.,* **105,** 113–120.

——, 1978: Mesocyclone evolution and tornadogenesis: Some observations. *Mon. Wea. Rev.,* **106,** 995–1011.

——, 1993: Tornadic thunderstorm characteristics determined with Doppler radar. *The Tornado: Its Structure, Dynamics, Prediction, and Hazards, Geophys. Monogr.,* No. 79, Amer. Geophys. Union, 143–159.

Brooks, H. E., C. A. Doswell III, and R. Davies-Jones, 1993: Environmental helicity and the maintenance and evolution of low-level mesocyclones. *The Tornado: Its Structure, Dynamics, Prediction, and Hazards, Geophys. Monogr.,* No. 79, Amer. Geophys. Union, 97–104.

——, ——, and R. B. Wilhelmson, 1994: The role of midtropospheric wind in the evolution and maintenance of low-level mesocyclones. *Mon. Wea. Rev.,* **122,** 126–136.

Brown, R. A., L. R. Lemon, and D. W. Burgess, 1978: Tornado detection by pulsed Doppler radar. *Mon. Wea. Rev.,* **106,** 29–39.

Browning, K. A., and R. J. Donaldson Jr., 1963: Airflow and structure of a tornadic storm. *J. Atmos. Sci.,* **20,** 533–545.

Burgess, D. W., and L. R. Lemon, 1990: Severe thunderstorm detection by radar. *Radar in Meteorology,* D. Atlas, Ed., Amer. Meteor. Soc., 619–647.

——, V. T. Wood, and R. A. Brown, 1982: Mesocyclone evolution statistics. Preprints, *12th Conf. on Severe Local Storms,* San Antonio, TX, Amer. Meteor. Soc., 422–424.

Chisholm, A. J., and H. H. Renick, 1972: The kinematics of multicell and supercell Alberta hailstorms. Alberta Hail Studies, 1972, Research Council of Alberta Hail Studies Rep. 72-2, 6 pp.

Church, C. R., J. T. Snow, G. L. Baker, and E. M. Agee, 1979:

Characteristics of tornado-like vortices as a function of swirl ratio: A laboratory investigation. *J. Atmos. Sci.*, **36,** 1755–1776.
Davies-Jones, R., 1973: The dependence of core radius on swirl ratio in a tornado simulator. *J. Atmos. Sci.*, **30,** 1427–1430.
——, and H. E. Brooks, 1993: Mesocyclogenesis from a theoretical perspective. *The Tornado: Its Structure, Dynamics, Prediction, and Hazards, Geophys. Monogr.*, No. 79, Amer. Geophys. Union, 105–114.
Donaldson, R. J., Jr., 1990: Foundations of severe storm detection by radar. *Radar in Meteorology*. D. Atlas, Ed., Amer. Meteor. Soc., 115–121.
Droegemeier, K. K., S. M. Lazarus, and R. Davies-Jones, 1993: The influence of helicity on numerically simulated convective storms. *Mon. Wea. Rev.*, **121,** 2005–2029.
Fujita, T. T., 1981: Tornadoes and downbursts in the context of generalized planetary scales. *J. Atmos. Sci.*, **38,** 1511–1534.
Gal-Chen, T., 1982: Errors in fixed and moving frame of references: Applications for conventional and Doppler radar analysis. *J. Atmos. Sci.*, **39,** 2279–2300.
Jischke, M. C., and M. Parang, 1974: Properties of simulated tornado-like vortices. *J. Atmos. Sci.*, **31,** 506–512.
Jorgensen, D. P., T. Matejka, and J. D. DuGranrut, 1996: Multi-beam techniques for deriving wind fields from airborne Doppler radars. *J. Meteor. Atmos. Phys.*, **59,** 83–104.
Klemp, J. B., 1987: Dynamics of tornadic thunderstorms. *Annu. Rev. Fluid Mech.*, **19,** 369–402.
——, and R. Rotunno, 1983: A study of the tornadic region within a supercell thunderstorm. *J. Atmos. Sci.*, **40,** 359–377.
Koch, S. E., M. DesJardins, and P. J. Kocin, 1983: An interactive Barnes objective map analysis scheme for use with satellite and conventional data. *J. Climate Appl. Meteor.*, **22,** 1487–1503.
Lee, W.-C., P. Dodge, F. D. Marks, and P. H. Hildebrand, 1994: Mapping of airborne Doppler radar data. *J. Atmos. Oceanic Technol.*, **11,** 572–578.
Lemon, L. R., 1980: Severe thunderstorm radar identification techniques and warning criteria. NOAA Tech. Memo. NWS NSSFC-3, 60 pp. [NTIS PB-231409.]
——, and C. A. Doswell III, 1979: Severe thunderstorm evolution and mesocyclone structure as related to tornadogenesis. *Mon. Wea. Rev.*, **107,** 1184–1197.
Leslie, L. M., 1971: The development of concentrated vortices: A numerical study. *J. Fluid Mech.*, **48,** 1–21.
Lewellen, W. S., 1976: Theoretical models of the tornado vortex. *Proc. Symp. on Tornadoes: Assessment of Knowledge and Implications for Man*, Lubbock, TX, Texas Tech University, 107–143.
Marwitz, J. D., 1972: The structure and motion of severe hailstorms. Part I: Supercell storms. *J. Appl. Meteor.*, **11,** 166–179.
McCaul, E. W., Jr., and M. L. Weisman, 1996: The dependence of simulated storm structure on variations in the shapes of environmental buoyancy and shear profiles. Preprints, *18th Conf. on Severe Local Storms*, San Francisco, CA, Amer. Meteor. Soc., 718–722.
Oye, R., C. Mueller, and S. Smith, 1995: Software for radar translation, visualization, editing, and interpretation. Preprints, *27th Conf. on Radar Meteorology*, Vail, CO, Amer. Meteor. Soc., 359–361.
Rasmussen, E. N., 1995: VORTEX operations plan. 141 pp. [Available upon request from National Severe Storms Laboratory, 1313 Halley Circle, Norman, OK 73069.]
——, J. M. Straka, R. P. Davies-Jones, C. A. Doswell, F. H. Carr, M. D. Eilts, and D. R. MacGorman, 1994: Verification of the Origins of Rotation in Tornadoes Experiment: VORTEX. *Bull. Amer. Meteor. Soc.*, **75,** 995–1006.
Ray, P. S., C. L. Ziegler, W. Bumgarner, and R. J. Serafin, 1980: Single- and multiple-Doppler radar observations of tornadic storms. *Mon. Wea. Rev.*, **108,** 1607–1625.
Rotunno, R., 1977: Numerical simulation of a laboratory vortex. *J. Atmos. Sci.*, **34,** 1942–1956.
——, 1984: An investigation of a three-dimensional asymmetric vortex. *J. Atmos. Sci.*, **41,** 283–298.
——, and J. B. Klemp, 1985: On the rotation and propagation of simulated supercell thunderstorms. *J. Atmos. Sci.*, **42,** 271–292.
Snow, J. T., 1982: A review of recent advances in tornado vortex dynamics. *Rev. Geophys. Space Phys.*, **20,** 953–964.
Sperow, K. S., 1995: Airborne Doppler analysis of the 18 February 1993 TOGA COARE squall line using a new analysis method: The two-step, second order Lax-Wendroff scheme. M.S. thesis, University of Oklahoma, 89 pp. [Available from School of Meteorology, University of Oklahoma, 100 E. Boyd, Norman, OK 73019.]
——, H. B. Bluestein, and T. Gal-Chen, 1995: Testing a Doppler analysis method: The two-step, second order Lax-Wendroff scheme. Preprints, *27th Conf. on Radar Meteorology*, Vail, CO, Amer. Meteor. Soc., 296–298.
Stout, G. E., and F. A. Huff, 1953: Radar records Illinois tornadogenesis. *Bull. Amer. Meteor. Soc.*, **34,** 281–284.
Straka, J. M., E. N. Rasmussen, and S. E. Fredrickson, 1996: A mobile mesonet for finescale meteorological observations. *J. Atmos. Oceanic Technol.*, **13,** 921–936.
Trapp, R. J., and B. F. Fiedler, 1995: Tornado-like vortexgenesis in a simplified numerical model. *J. Atmos. Sci.*, **52,** 3757–3778.
——, and R. Davies-Jones, 1997: Tornadogenesis with and without a dynamic pipe effect. *J. Atmos. Sci.*, **54,** 113–133.
Wakimoto, R. M., and N. T. Atkins, 1996: Observations on the origins of rotation: The Newcastle tornado during VORTEX 94. *Mon. Wea. Rev.*, **124,** 384–407.
——, and C. Liu, 1998: The Garden City, Kansas, storm during VORTEX 95. Part II: The wall cloud and tornado. *Mon. Wea. Rev.*, **126,** 393–408.
Ward, N. B., 1972: The exploration of certain features of tornado dynamics using a laboratory model. *J. Atmos. Sci.*, **29,** 1194–1204.
Weisman, M. L., and J. B. Klemp, 1982: The dependence of numerically simulated convective storms on vertical wind shear and buoyancy. *Mon. Wea. Rev.*, **110,** 504–520.